HHS Public Access

Author manuscript

Med Image Comput Comput Assist Interv. Author manuscript; available in PMC 2017 October 16.

Published in final edited form as:

Med Image Comput Comput Assist Interv. 2017 September ; 10433: 584–592. doi: 10.1007/978-3-319-66182-7_67.

FOD Restoration for Enhanced Mapping of White Matter Lesion Connectivity

Wei Sun[1], **Lilyana Amezcua**[2], and **Yonggang Shi**[1,★]

[1]Laboratory of Neuro Imaging, USC Stevens Neuroimaging and Informatics Institute, Keck School of Medicine, University of Southern California, Los Angeles, USA

[2]Multiple Sclerosis Comprehensive Care Center, Keck School of Medicine, University of Southern California, Los Angeles, USA

Abstract

To achieve improved understanding of white matter (WM) lesions and their effect on brain functions, it is important to obtain a comprehensive map of their connectivity. However, changes of the cellular environment in WM lesions attenuate diffusion MRI (dMRI) signals and make the robust estimation of fiber orientation distributions (FODs) difficult. In this work, we integrate techniques from image inpainting and compartment modeling to develop a novel method for enhancing FOD estimation in WM lesions from multi-shell dMRI, which is becoming increasingly popular with the success of the Human Connectome Project (HCP). By using FODs estimated from normal WM as the boundary condition, our method iteratively cycles through two key steps: diffusion-based inpainting and FOD reconstruction with compartment modeling for the successful restoration of FODs in WM lesions. In our experiments, we carry out extensive simulations to quantitatively demonstrate that our method outperforms a state-of-the-art method in angular accuracy and compartment parameter estimation. We also apply our method to multi-shell imaging data from 23 multiple sclerosis (MS) patients and one LifeSpan subject of HCP with WM lesion. We show that our method achieves superior performance in mapping the connectivity of WM lesions with FOD-based tractography.

1 Introduction

White matter (WM) lesions often occur in normal aging with vascular origins [1] or neurological disorders such as multiple sclerosis (MS) [2], but their impact on brain function often are not well understood. A comprehensive map of their connectivity to cortical and sub-cortical regions will not doubt improve our study and management these lesions [3]. Diffusion MRI(dMRI) has played a central role for the *in vivo* mapping of structural connectivity in human brain. The presence of extra-axonal fluid in the WM lesion due to pathology, however, dramatically attenuates the dMRI signals and reduces the signal to noise ratio (SNR), making it challenging to recover the underling fiber orientations and map lesion connectivity [4]. The emergence of multi-shell dMRI for connectome imaging studies[5]

★This work was in part supported by the National Institute of Health (NIH) under Grant R01EB022744, P41EB015922, U01EY025864, U01AG051218, P50AG05142.

allows the incorporation of compartment models and holds promise for more robust analysis of lesion connectivity, but the loss of SNR still poses serious challenges even for these advanced analysis techniques.

In this work we propose a novel method for more accurate estimation of fiber orientation distribution (FOD) in WM lesions from multi-shell dMRI. The main idea is the effective combination of an inpainting and estimation step with an operator splitting scheme [6]. For the processing of T1 or T2-weighted images in MS research, inpainting methods were applied to improve the robustness of image registration and segmentation [7–9]. Our work is novel in that we are processing high dimensional FODs from multi-shell diffusion imaging and we aim for the restoration of both the shape and magnitude of the FODs. We also incorporate the diffusion-based inpainting with data-driven restoration to improve the overall estimation of the FODs. In our experiments, we demonstrate our method on both simulations and multi-shell imaging data from a cohort of 23 MS patients and one LifeSpan subject from HCP [5]. In comparisons with a state-of-the-art method for FOD modeling from multi-shell imaging data [10], we show that our method achieves better performance for FOD estimation in WM lesions and produces more complete mapping of lesion connectivity with tractography.

2 Method

In Figure 1, we provide an overview of the proposed method with a 2D illustration. The normal tissue, ventricle and lesion voxels are labelled in white, black and grey, respectively. As a first step of our method, we compute the FODs for the whole brain mask using the multi-compartment algorithm in [10]. A subset of FODs within normal tissue are fixed as boundary condition (marked in yellow) for later inpainting iterations. Next, the magnitude of FODs in the lesion region are initialized from the fixed boundary and surrounding voxels in normal tissue to interior voxels. For example, the red dot in Figure 1 highlights one boundary lesion voxel with at least one of its four nearest neighbor voxels (marked in blue) belonging to normal tissue. The magnitude of the FOD at this lesion voxel is initialized as the weighted mean of FODs from neighboring voxels in normal tissue inside an image patch (marked in green) centered at the lesion voxel. After the initialization for all voxels are completed, we reconstruct the FODs in the WM lesion by iteratively cycling through an inpainting and restoration step until a stopping criteria is met. The inpainting step propagates information of FODs from the normal tissue to voxels inside the WM lesion, while the restoration step integrates this regularity with the dMRI signal for the calculation of the FOD. Next we will present the details of this algorithm.

2.1 Multi-compartment Modeling for FOD Reconstruction

Let $\mathcal{B} \subset \mathbb{R}^D$ denotes a brain mask where D is image dimension. Let a vector $s_p(b)$ denote the diffusion imaging signal at voxel p with a b-value b and from N gradient directions where $p \in \mathcal{B}$. Following the multi-compartment model in [10], in this work $s_p(b)$ is represented as three compartment models: intra-axonal compartment with (i.e., a stick kernel), extra-axonal compartment (i.e., a sphere model) and the DOT model with negligible diffusion. Then $s_p(b)$ is defined as:

$$s_p(b)=Ax+\alpha\beta+\gamma\rho+\zeta, \quad (1)$$

where the matrix A represents the spherical convolution of the FOD and a stick kernel, x is the vector of spherical harmonics (SPHARM) coefficients for the FOD, $\beta = [e^{-b_1\lambda_{iso}} e^{-b_2\lambda_{iso}} \cdots e^{-b_N\lambda_{iso}}]^T$ with isotropic diffusivity λ_{iso}, $\rho = [11 \cdots 1]^T$ with length N, and ζ is the vector of noise. Therefore, we can define and minimize the following energy function which consists of a data fidelity term and an L_1 sparsity penalty term of FOD:

$$\begin{aligned} &\text{minimize} \quad E(x,\alpha,\lambda_{iso},\gamma)=\tfrac{1}{2}\left\| s_p-[A,\ \beta,\ \rho]\begin{bmatrix} x \\ \alpha \\ \gamma \end{bmatrix}\right\|^2+\xi Ix \\ &\text{subject to} \quad Ix+\alpha+\gamma=1,\ C_M x\geq 0,\ \alpha\geq 0,\ \lambda_{iso}\geq 0,\ \text{and}\ \gamma\geq 0. \end{aligned} \quad (2)$$

where ξ represents the weighting coefficient of sparsity term. Because the integral of all SPHARM basis with order $l \geq 1$ is zero, we have the matrix representation of the sparsity term with $I=[\sqrt{4\pi},\ 0, \cdots, 0]$ and the volume fractions of all three compartments should satisfy the normalization constraint $Ix + \alpha + \gamma = 1$. C_M denotes an adaptively computed constraint matrix to guarantee the nonnegativity of FOD [10]. To estimate the unknown x, α, λ_{iso}, γ, a coordinate descent algorithm is employed to optimize them iteratively using a quadratic programming step and a gradient descent step.

2.2 Initialization of Lesion FOD

Assume we have a well-defined lesion mask $\mathcal{L} \subset \mathcal{B}$ and ventricle mask $\mathcal{V} \subset \mathcal{B}$. For $q \in \mathcal{L}$, let $\mathcal{P}_q$ be an image patch centered at q with $h^D - 1$ voxels (i.e., voxel q is excluded). Let $x' = x/\|x\|$ stand for the normalized x where $\|\cdot\|$ is the L_2-norm. This means we can measure the similarity of normalized SPHARMs coefficients (i.e., FOD shape) regardless the FOD size. The dissimilarity measure $\mathrm{Diff}(q,n)=\|x'_q - x'_n\|$ computes the difference of FOD shapes between voxel q and $\forall n \in \{n: n \in \mathcal{P}_q \cap \mathcal{B} \wedge n \notin \mathcal{L} \cup \mathcal{V}\}$ (i.e., all voxels of normal tissue within image patch $\mathcal{P}_q$). We select a subset of $\mathcal{P}_q$:

$$\mathcal{P}_q^*=\{n^*: n^* \in \mathcal{P}_q \wedge D(q,n^*) \leq T_{sim}\} \quad (3)$$

where T_{sim} is the threshold of similarity and Eq. (3) selects $\mathcal{P}_q^*$ with the differences of FOD shapes equal or smaller than T_{sim}. Then $\mathcal{M} \subseteq \mathcal{P}_q^*$ which consists of the first m largest $\|x_n^*\|$ (i.e., FOD size) can be chosen from $\mathcal{P}_q^*$ where $m \leq \left|\mathcal{P}_q^*\right|$ and $|\cdot|$ is the cardinality (i.e., number of voxels). This means the adjacent FODs which have similar shapes with x_q will be selected and the voxels which are very close to the gray matter are expected to be excluded because of their small FOD sizes. Let w denote a vector consisting of intra-axonal fraction Ix, extra-axonal fraction α, DOT model fraction γ, and isotropic diffusivity λ_{iso}. Then the weighted mean for voxel q is computed as

$$\overline{w}_q=\sum_{i\in\mathcal{M}}\left(\eta(\|x_q^{'}-x_i^{'}\|)w_i\right)/\sum_{i\in\mathcal{M}}\eta(\|x_q^{'}-x_i^{'}\|), \quad (4)$$

where $\eta(\|\cdot\|)$ is a Gaussian PDF with mean zero and standard deviation σ_w. With $\bar{w}_q$, we can calculate the recovery weighting factors through element-wise division of $\bar{w}_q$ by w_q and then multiply the corresponding factors back to x_q, a, γ and λ_{iso} to enlarge the FOD magnitude of voxel q.

After the initialization of voxel q, it is temporarily removed from lesion mask $\mathcal{L}$ and will be regarded as a normal voxel in the consequent initializations of other lesion voxels. The entire initialization process will end when $\mathcal{L}$ = Ø.

2.3 Inpainting and Restoring Lesion FOD

After the initialization, the magnitudes of lesion FODs are recovered. However, the FOD shape of lesion voxel has still been deteriorated due to the poor dMRI signal of lesion region. In addition, we still need a buffing process to smooth the initialized compartment fractions of lesion FOD with its adjacent FODs. First, an anisotropic inpainting step is employed to bring the FOD regularity of fixed boundary condition to inner lesion region. Second, we minimize a new energy function derived from Eq. (2) with an additional spatial regularization term to balance the fidelity between initialized diffusion signal and anisotropic smoothing. Motivated by the operator splitting optimization [6], an iterative approach for the inpainting and restoration of lesion FOD is proposed in this work. With operator splitting, the two steps are executed iteratively until reaching a stopping criterion.

For the inpainting step, we assume the SPHARMs coefficients x_q, extra-axonal fraction a_q and DOT model fraction γ should be similar among the surrounding FODs. We follow the anisotropic diffusion in [11] to implement our high dimensional smoothing algorithm. As shown in Figure 1, one center voxel (marked as red dot) has 4 nearest-neighbor voxels (marked as blue dots) in 2D case. For 3D data, we apply the same scheme to one center voxel surrounded by 6 nearest-neighbor voxels. Let us denote $\varepsilon(q)=[\,\|x_q\|\cdot x_q^{'},\,\alpha_q,\,\gamma_q]^T$. Then we can construct a vector $\upsilon(q)=[\,\|x_q\|,\,x_q^{'},\,\alpha_q,\,\gamma_q]^T$ where $\upsilon^1(q)=\|x_q\|$, $\upsilon^2(q)=x_q^{'}$, $\upsilon^3(q)=a_q$ and $\upsilon^4(q)=\gamma_q$. By this means, the normalized $x_q^{'}$ and its norm $\|x_q\|$ are separated as two elements of $\upsilon(q)$. The $\upsilon(n_j)$ of one nearest neighbor n_j can be defined similarly as $[\,\|x_{nj}\|,\,x_{nj}^{'},\,\alpha_{nj},\,\gamma_{nj}]^T$. Then the anisotropically smoothed $\upsilon_k^{(i)}(q)$ is computed as:

$$\overline{\upsilon}_k^i(q)=\upsilon_k^i(q)+\tau\sum_{j=1}^{4}g(\|\upsilon_k^i(q)-\upsilon_k^i(n_j)\|)(\upsilon_k^i(q)-\upsilon_k^i(n_j)), \quad (5)$$

where $k\in[0,K]$ represents the iteration number, τ is the Gaussian diffusion duration. The anisotropic weight is $g(\|\cdot\|)=e^{-(\|\cdot\|/\sigma_s)^2}$ where σ_s controls the effect range of anisotropic

smoothing. Note that the smoothed SPHARMs coefficients $\overline{x}_q = \overline{v}_k^1(q) \cdot \overline{v}_k^2(q)$ and then we have the smoothed $\bar{\varepsilon}_k(q) = [\bar{x}_q, \bar{a}_q, \bar{\gamma}_q,]^T$.

Next, the energy function with auxiliary term is minimized for all $q \in \mathcal{R}$:

$$E_{k+1}^*(q) = \frac{1}{2}\|\hat{s}_q - [A, \beta, \rho]\ \varepsilon_{k+1}(q)\|^2 + \xi Ix(q) + \frac{\omega}{2\tau}\|\varepsilon_{k+1}(q) - \bar{\varepsilon}_k(q)\|^2, \quad (6)$$

where $\hat{s}_q$ is the initialized diffusion signal with enlarged FOD size. The last term in Eq. (6) introduces the anisotropic inpainting step to the optimization. Because less weight should be put on the auxiliary term if it is overly smoothed, the weight of last term is inversely proportional to τ in Eq. (5).

3 Experiments

3.1 Simulation

In this section, we applied our method to both simulated and *in vivo* multi-shell dMRI data. We compare out results with the multi-compartment method in [10], which we designate as the baseline method in our experiments. For real data, WM lesion masks were manually annotated from T2-weighted MRI, and the ventricle masks were obtained by manually correcting automated segmentation results. The weighting coefficient of sparsity term ξ was fixed to 0.2. The diffusion time τ was chosen as 0.15 for numerical stability. The patch size h in FOD initialization was 5 and 9 for simulation and real data, respectively. The threshold T_{sim} for FOD similarity was 0.7. In Eq. (4) the cardinality m was fixed to 3. The standard deviation σ_w in Eq. (4) was 0.4. For anisotropic regularization, σ_s in Eq. (5) was fixed to 0.5. The weighting factor ω in Eq. (6) was 20. We fixed the iteration numbers $K = 20$ on simulated data and $K = 10$ on real data.

In our simulation, we used a multi-shell diffusion protocol from the LifeSpan project of HCP that consists of b-values $1500 s/mm^2$ and $3000 s/mm^2$ and 98 gradient directions. For the normal voxel, the simulated intra-axonal, extra-axonal, and trapped water fractions were fixed as: 0.35, 0.5 and 0.15, respectively. Because the water diffusion in extra-axonal compartment should be lower than the intra-axonal compartment $\lambda_{||} = 0.0017 mm^2/s$, we picked the diffusivity of extra-axonal compartment as $\lambda_{iso} = 0.0012 mm^2/s$. Figures 2(a) and (e) show the two ground truth fiber patterns in the simulation. Figure 2(a) consists of signal fiber direction at 90°. Figure 2(e) contains two fiber directions at 90° and 60°. To simulate a 3×3 lesion region (marked in red) located at the center of Figures 2(a) or (e), we modified the intra-axonal, extra-axonal, and trapped water fractions to 0.07, 0.7 and 0.23, respectively. Rician noise was added so that dMRI data within lesion region have an SNR = 3.

Figures 2(b) and (f) show the baseline reconstructions of the simulated FOD without applying the proposed approach. Figures 2(c) and (g) present the results after the initialization of lesion FODs, where we can see the magnitudes of FODs were recovered, but there are still false and random rotations in fiber directions. As shown in Figures 2(d) and (h), the results achieved by the proposed approach successfully restored the lesion FODs

with proper shapes and magnitudes. To quantitatively measure the reconstruction accuracy, we computed the *average angular error* (AAE) [10] for all the 3×3 lesion voxels. The AAE of each lesion voxel are summarized in Figure 3(a). Compared with the baseline results, the proposed method clearly improved the AAE accuracy. For the simulation data, the ground truth of extra-axonal fraction is 0.5. Thus we can compute the difference of the reconstructed extra-axonal fraction with the ground truth. From Figure 3(b), we can see the proposed approach also reduced the errors in measuring the volume fraction of the extra-axonal compartment. Figure 3(c) shows the convergence curve of the proposed approach during the optimization of Eqs. (5) and (6). The results con-firmed that the proposed algorithm converged to a local minima. It also shows that practically 10 iterations, which we will use for real data, would be a good balance between computational cost and reconstruction accuracy.

3.2 Multi-shell Imaging Data of Human Brains

We acquired *in vivo* data from 23 patients with multiple sclerosis (MS). The imaging protocol contains two shells with b-values $1000 s/mm^2$, $2000 s/mm^2$ and 45 gradient directions. In addition, the proposed approach was also applied to the multi-shell imaging of a HCP LifeSpan subject whose brain contains WM lesions due to aging.

The reconstruction results from an MS patient are first shown in Figure 4. Figure 4(a) shows the mask of WM lesions. In Figure 4(b) the FODs from the baseline method show strong attenuation due to the WM lesion. In contrast, Figure 4(c) presents the results achieved by the proposed approach. We can see the restored FODs demonstrate high coherence with the surrounding FODs in normal WM. Figures 4(d) and (e) show the track-density imaging (TDI) [12] results computed from 1 million fiber tracts by the MRTrix tool[13]. Due to the WM lesion, we can observe a clear loss of the fiber connectivity in Figure 4(d). As shown in Figure 4(e), the proposed approach restored the lost fiber connectivity.

To further compare the effect of different FOD reconstruction results on studying lesion connectivity, we ran FOD-based tractography from a randomly selected voxel around lesion center for each subject. The same tractography parameters of MRTrix were used for all subjects and methods: curvature=1.5; FOD threshold=0.05; maximum number of tracts = 2000. Figure 5(a) shows three representative results of the fiber tracking based on the FOD computed by the baseline (see first row) and proposed (see second row) method. In contrast to the baseline results, the proposed method resulted in more complete reconstruction of lesion connectivity. To quantitatively measure the performance on each subject, we used TrackVis [14] to compute the tract volume. Figure 5(b) plots the results of tract volume on each subject, where the first 23 subjects are MS patients and the 24th subject is from the LifeSpan project of HCP. We can see the proposed approach improved the tract volume in all the subjects as consistent with the individual examples shown in Figure 5(a).

4 Conclusion

In this work we propose a novel approach for the restoration of FODs within WM lesions. Results from our simulation and real data demonstrate the potential of the proposed method

for more robust mapping of WM lesion connectivity. For future work, we will validate our method on WM lesions from both vascular origin and multiple sclerosis in clinical studies.

References

1. Breteler MM, van Amerongen NM, van Swieten JC, Claus JJ, Grobbee DE, van Gijn J, Hofman A, van Harskamp F. Cognitive correlates of ventricular enlargement and cerebral white matter lesions on magnetic resonance imaging. the rotterdam study. Stroke. 1994; 25(6):1109–15. [PubMed: 8202966]
2. Dutta R, Trapp BD. Pathogenesis of axonal and neuronal damage in multiple sclerosis. Neurology. 2007; 68(22 suppl 3):S22–S31. [PubMed: 17548565]
3. Liang Y, Sun X, Xu S, Liu Y, Huang R, Jia J, Zhang Z. Preclinical cerebral network connectivity evidence of deficits in mild white matter lesions. Frontiers in Aging Neuroscience. 2016; 8:27. [PubMed: 26924981]
4. Wang Y, Wang Q, Haldar JP, Yeh FC, Xie M, Sun P, Tu TW, Trinkaus K, Klein RS, Cross AH, Song SK. Quantification of increased cellularity during in ammatory demyelination. Brain. 2011; 134(12):3590. [PubMed: 22171354]
5. Van Essen DC, Ugurbil K, Auerbach E, Barch D, Behrens T, Bucholz R, Chang A, Chen L, Corbetta M, Curtiss SW, et al. The Human Connectome Project: A data acquisition perspective. NeuroImage. 2012; 62(4):2222–2231. [PubMed: 22366334]
6. Zhang X, Burger M, Bresson X, Osher S. Bregmanized nonlocal regularization for deconvolution and sparse reconstruction. SIAM J Img Sci. 2010; 3(3):253–276.
7. Chard DT, Jackson JS, Miller DH. Wheeler-Kingshott, C.A. Reducing the impact of white matter lesions on automated measures of brain gray and white matter volumes. J Magn Reson Imaging. 2010; 32(1):223–228. [PubMed: 20575080]
8. Sdika M, Pelletier D. Nonrigid registration of multiple sclerosis brain images using lesion inpainting for morphometry or lesion mapping. Hum Brain Mapp. 2009; 30(4):1060–1067. [PubMed: 18412131]
9. Prados, F., Cardoso, MJ., MacManus, D., Wheeler-Kingshott, CA., Ourselin, S. MICCAI. Springer; 2014. A modality-agnostic patch-based technique for lesion filling in multiple sclerosis; p. 781-788.
10. Tran G, Shi Y. Fiber orientation and compartment parameter estimation from multi-shell diffusion imaging. IEEE T Med Imaging. 2015; 34(11):2320–2332.
11. Perona P, Malik J. Scale-space and edge detection using anisotropic diffusion. IEEE T Pattern Anal. 1990; 12(7):629–639.
12. Calamante F, Tournier JD, Jackson GD, Connelly A. Track-density imaging (TDI): Super-resolution white matter imaging using whole-brain track-density mapping. NeuroImage. 2010; 53(4):1233. [PubMed: 20643215]
13. Tournier J, Calamante F, Connelly A, et al. MRtrix: Diffusion tractography in crossing fiber regions. Int J Imag Syst Tech. 2012; 22(1):53–66.
14. Wang R, Benner T, Sorensen AG, Wedeen VJ. Diffusion toolkit: a software package for diffusion imaging data processing and tractography. Proc Intl Soc Mag Reson Med. 2007; 15

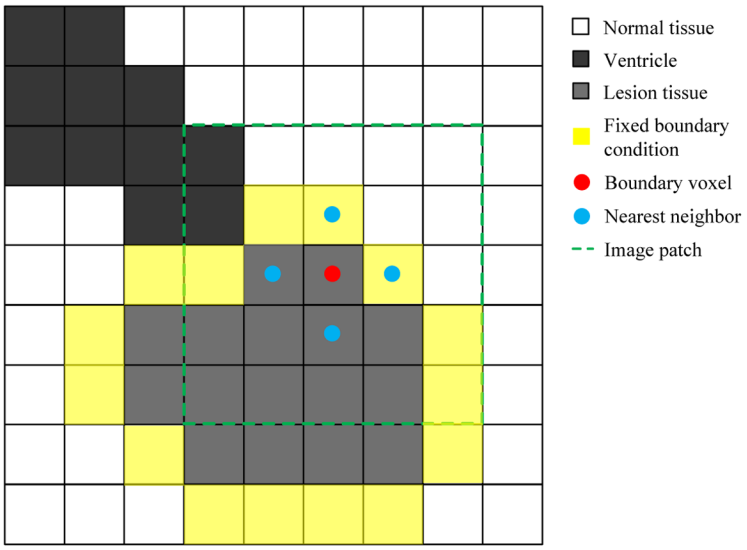

Fig. 1.
Illustration of the proposed FOD restoration approach for white matter lesion.

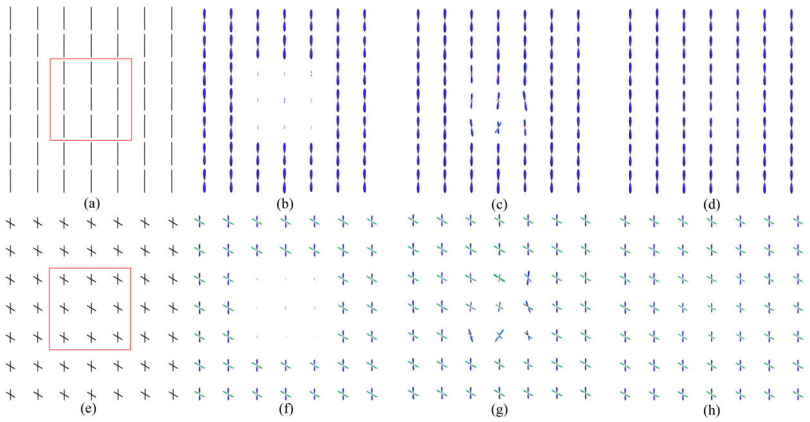

Fig. 2.

FOD on simulated data: (a) and (e) simulated fiber directions; (b) and (f) baseline; (c) and (g) initialized; (d) and (h) proposed.

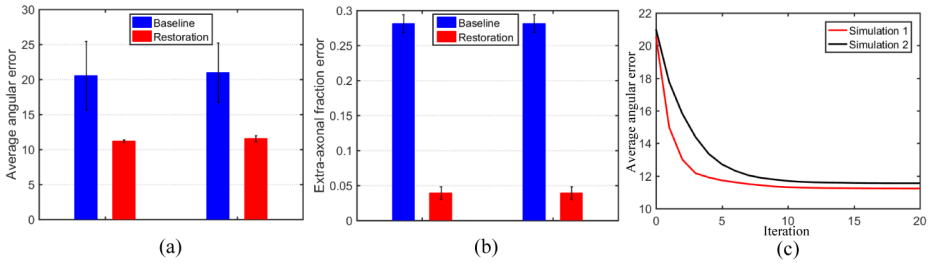

Fig. 3.

Reconstruction results on simulated data: (a) mean average angular error with standard deviation; (b) mean extra-axonal fraction error with standard deviation (c) convergence curves.

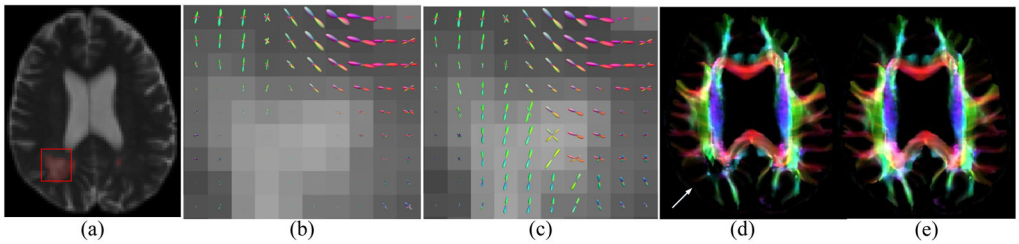

Fig. 4.

FOD and TDI results from one subject. Results from one ROI shown in (a) are plotted in (b) and (c). (b) and (d) are baseline results. (c) and (e) are the results achived by our approach.

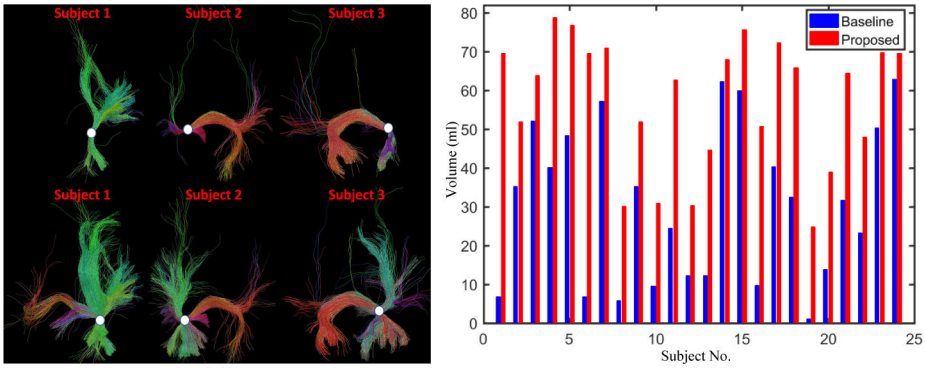

(a) (b)

Fig. 5.

Fiber tracts constructed from random single seed voxels within lesion regions. The white disk indicates the seed location. (a) the first and second rows are the results of baseline and proposed approach, respectively. (b) tract volume (ml) on each subject.